Optimizing Spatial Channel Networks (SCNs) in Hierarchical Optical Cross-Connect (HOXC) architectures: Impact of wavelength switching granularity on performance

Optimizing Spatial Channel Networks (SCNs) in Hierarchical Optical Cross-Connect (HOXC) architectures: Impact of wavelength switching granularity on performance

Weichang Zheng [a], Jinke Li [a], Ming Ke [a], Mingcong Yang [b], Yu Zheng [c], Chenxiao Zhang [d], Qiang Liu [a], Yongbing Zhang [c], Kun Yang [a]

[a] Yangtze Delta Region Institute (Quzhou), University of Electronic Science and Technology of China, No. 1 Chengdian Road, Kecheng District, Quzhou, 324300, Zhejiang, China

[b] ZTE Wuhan R&D Center, No. 422 Xinhua Road, Jianghan District, Wuhan, 430015, Hubei, China

[c] Graduate School of Systems and Information Engineering, University of Tsukuba, 1 Chome-1-1 Tennodai, Tsukuba, 3050005, Amakubo, Japan

[d] KDDI Corporation, 3-10-10 Garden Air Tower, Chiyoda-ku, 1028460, Tokyo, Japan

Abstract

The increasing demand for network bandwidth highlights the critical need to enhance optical transmission systems. Utilizing the entire C-band for a single optical channel(OCh) eliminates the requirement for wavelength switching, prompting the emergence of spatial channel networks (SCNs). SCNs transform the optical layer into hierarchical spatial division multiplexing (SDM) and wavelength division multiplexing (WDM) layers through the implementation of hierarchical optical cross-connects (HOXCs). A HOXC comprises a spatial channel cross-connect (SXC) for spatial bypass switching and multiple wavelength cross-connects (WXCs) for wavelength channel switching, ensuring efficient optical transmission. Therefore, the design of the HOXC plays a pivotal role in determining both the device cost and network performance in SCNs. This study investigates the impact of wavelength switching granularity on core-selective switch (CSS)-based HOXC architectures. We propose an adaptive dynamic Routing, Spatial Channel, and Spectrum Assignment (RSCSA) algorithm to solve routing and resource allocation problems in SCNs. By examining SCN designs with varying wavelength switching granularities, we assess the overall network deployment cost, considering both network throughput and spectrum resource utilization. Our findings indicate that adjusting the granularity of wavelength switching in SCNs can significantly affect device costs and performance, highlighting the importance of identifying an optimal SCN design that strikes a balance between these factors. These insights offer valuable guidance for the practical planning and management of future SCN deployments.

Keywords: Spatial Channel Network (SCN) Spatial bypass CSS-based HOXC Wavelength switching granularity Device cost and network performance

1. Introduction

With the router interface speed's estimated compound annual growth rate of 40% [1], the demand for higher bandwidth capacity in optical transport systems is poised to reach Pbps levels. This substantial increase in traffic demand highlights the need for innovative systems capable of expanding bandwidth. As predicted in [2], future demands for terabit-level requests, such as a single 10 Tb/s dual-polarization quadrature phase shift keying (DP-QPSK) optical channel, are expected to consume the entire 4.4 THz spectrum resource within the C-band. This complete utilization of the C-band spectrum for a single optical channel, thereby obviating the need for wavelength switching, paves the way for the adoption of a novel optical transport network (OTN) architecture, known as spatial channel networks (SCNs) [2]. SCNs are designed to offer a cost-efficient solution to address the challenges posed by the impending massive spatial division multiplexing (SDM) era. They evolve the optical layer into a hierarchical structure, integrating SDM and wavelength division multiplexing (WDM) layers, and leveraging the advantages of both SDM and WDM technologies.

In recent years, SDM has been considered a feasible solution to break through the capacity barriers of existing OTNs based on single-mode fibers (SMFs). While SDM technology considerably expands network capacity by exploiting the spatial dimensions of optical fibers, it alone is not sufficient to support Pbps-level transmission. Introduced in 2019, SCNs offer a framework that addresses performance bottlenecks in SDM-based transmission systems. The primary feature of SCN is the hierarchical separation of the optical layer into SDM and

WDM layers. This distinguishes SCNs from other optical networking technologies and is crucial for efficient data transmission. In SCNs, two main technologies–spatial bypass and spectral grooming–enable optical transmission capable of accommodating a wide range of traffic demands [3].

Spatial bypass technology in SCNs draws inspiration from the concept of optical bypass in WDM systems, which can be traced back to the early 2000s [4]. During that period, the OTN standard was proposed as an alternative to the synchronous digital hierarchy (SDH) [5] as the interface to the optical layer. WDM systems require an extensive array of optical and electrical components at each node, such as optical channel data unit cross-connects and optical transceivers. This complexity necessitates electronic processing for all incoming and outgoing traffic at each node, resulting in significant costs and resource wastage. To overcome this, reconfigurable optical add/drop multiplexers (ROADMs) or WDM add/drop multiplexers are introduced. These devices allow individual wavelengths to either undergo electronic processing or optically bypass the electronic components of a node [6]. In the forthcoming era dominated by massive SDM, wavelength switching is not required for the requests transmitted using the entire C-band spectrum [1,7]. Inspired by optical bypass in WDM systems, spatial bypass technology has been developed for SCNs. Enabled by spatial channel cross-connects (SXCs), this technology allows for end-to-end routing without the need for wavelength switching, offering a more cost-effective and resource-efficient solution.

Another key technology in SCNs is spectral grooming [8–10], a strategy widely acknowledged for its effective allocation and management of spectrum resources. Spectral grooming serves as an advanced end-to-end multiplexing technique, aggregating traffic demands at both intermediate and terminal nodes [11,12]. It is characterized by two main features: channel aggregation and dynamic spectrum assignment. Channel aggregation combines multiple lower-speed channels into a single higher-speed channel, minimizing the need for optical transceivers and improving spectrum utilization. On the other hand, dynamic spectrum assignment allows for the flexible allocation of optical channels based on varying bandwidth requirements, thereby optimizing the use of available spectrum resources.

In SCNs, an innovative ROADM architecture known as hierarchical optical cross-connect (HOXC) has been introduced. This architecture takes advantage of spatial bypass and spectral grooming, leading to two benefits [13]. First, by integrating a SXC along with the appropriate number of wavelength cross-connects (WXCs), HOXC reduces the per-node cost. Second, HOXC enables optical signals to bypass the WDM layer through SXCs, eliminating the need for photoelectric conversion and passing through multiple devices. This reduces signal loss, thereby extending the optical reach over longer distances. These benefits further emphasize the critical role of HOXC architecture design for SCNs.

In this paper, we explore how wavelength switching granularity affects the performance of SCNs in the CSS-based HOXC architecture. Wavelength switching granularity is defined by the proportion of spatial lanes (SLs) supporting wavelength switching, which is directly linked to the quantity of WXCs deployed. This factor crucially shapes the SXC architecture and, by extension, the overall design of HOXC. To evaluate the influence of wavelength switching granularity on HOXC architectures, we address the dynamic routing, spatial channel, and spectrum assignment (RSCSA) problems, taking into account device cost, network throughput, and resource utilization.

The main contributions of this paper can be summarized as follows: (1) We propose a novel method to design the architecture of SCNs, focusing on identifying the optimal wavelength switching granularity, which we define as the proportion of SLs supporting wavelength switching. Our dynamic RSCSA solutions reveal that increasing the proportion of SLs supporting wavelength switching improves routing flexibility at the expense of increased device cost and reduced resource utilization. This is attributed to the need for more WXCs and transceivers, which, although they offer greater routing flexibility, necessitate additional switching guard bands (GBs) and incur higher costs. (2) We conduct a comprehensive analysis of SCN architectures, evaluating how varying levels of wavelength switching granularity affect device cost, network throughput, and resource utilization. Our analysis aims to identify an optimal trade-off, providing network operators with practical insights for network planning and management. (3) We detail the architecture of a HOXC and clarify how various components of the HOXC interrelate. (4) We develop an adaptive dynamic RSCSA algorithm to solve routing and resource assignment problems in SCNs. Depending on the traffic demand level of requests, we employ different types of SChs to maximize the utilization of SLs and spectrum resources, thereby improving the success rate of routing. (5) We observe that device cost is directly proportional to wavelength switching granularity. Network throughput increases first and then decreases as the granularity rises, and resource utilization is inversely proportional to the granularity. Notably, a proportion of 0.2 demonstrates effective performance in balancing device cost against network throughput.

The rest of this paper is organized as follows: Section 2 offers an overview of existing research works related to SCNs. In Section 3, we describe the basic features of SCNs, discuss the advantages and challenges of introducing SCN technology, introduce our proposed HOXC architecture, and present the model for estimating device cost. Section 4 proposes a detailed description of our proposed adaptive dynamic RSCSA algorithm. Section 5 discusses the network topologies and the assumptions of our simulation experiments. Section 6 details the performance metrics of device cost, network throughput, and resource utilization and analyzes the results of each metric. Finally, in Section 7, we conclude the paper and provide a brief outlook on our future works.

2. Related works

Over the past decade, many research works have been conducted to explore and discuss various topics related to SCNs. The concept of SCN was first proposed in [14,15] by Professor Masahiko Jinno in 2018. In [2], the authors gave a comprehensive introduction to the features of SCNs and discussed the opportunities and challenges of introducing SCNs. [16] proposed the core selective switch (CSS) architecture for SCNs and verified its feasibility. [17] designed and prototyped a 5-core 1 × 6 CSS-based HOXC to demonstrate spatial bypass and spectral grooming. In [7], the authors conducted a proof of concept demonstration to showcase the feasibility of SCNs utilizing low-loss HOXCs and 4-core multicore fiber (MCF) links. In [18], the authors presented the principle, design, and prototyping of a free-space-optics-based CSS specifically developed for SCNs. In [3], a technical analysis was conducted on SCNs, considering various HOXC architectures. Additionally, the authors developed a routing and SDM/WDM multilayer resource assignment (RSWA) heuristic aimed at minimizing the number of required SLs. In [19], the authors presented feasibility demonstrations of the SCN architecture, highlighting its ability to enhance the flexibility and functionality of spatial channel networking. In [20], the authors proposed an integer linear programming (ILP) model and a heuristic algorithm to solve the RSCSA problem in SCNs. [21] presented a novel architecture design of CSS based on a two-dimensionally arranged microlens-based MCF collimator array and a micro-electromechanical systems (MEMS) mirror array. In [22], the authors proposed a single MCF bidirectional SCN that efficiently accommodates asymmetric traffic. [23] focused on solving the routing, modulation format, spatial lane, and spectrum block assignment (RMSSA) problem in static SD-SCNs.

Table 1 presents a comparative analysis of associated technologies examined in previous works and this research. It evaluates the presence of SXC and WXC across different configurations, including CSS-based and matrix switch (MS)-based for SXC, as well as R&S-based and B&S-based for WXC. Our research stands out with a dynamic approach, introducing variable wavelength switching granularity (W ratio) and fixed add/drop ratio (A ratio), unlike those observed in prior works. This is the first work that considers dynamic routing and resource allocation in SCNs.

Table 1
Comparison of previous works and our research.

Ref.	Sce.	SXC		WXC		W ratio	A ratio
		CSS	MS	R&S	B&S		
[2]	–	✓	✓	✓		fixed	fixed
[3]	–	✓	✓		✓	fixed	fixed
[7]	–	✓	✓	✓	✓	fixed	fixed
[14]	–	✓		✓		fixed	fixed
[15]	–	✓	✓	✓		fixed	fixed
[16]	–	✓		✓		fixed	fixed
[17]	–	✓		–	–	fixed	fixed
[18]	–	✓		✓		fixed	fixed
[19]	–	✓			✓	fixed	fixed
[20]	static	✓		–	–	fixed	fixed
[21]	–	✓			✓	fixed	fixed
[22]	–	✓			✓	fixed	fixed
[23]	static	–	–	–	–	fixed	fixed
This work	dynamic	✓		✓		variable	fixed

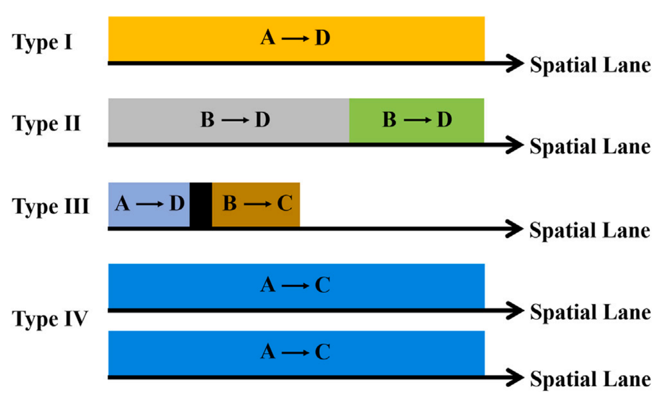

Fig. 1. Different types of SChs.

3. Spatial channel networks

To keep pace with the upcoming era of massive SDM, the proposed SCN is considered a promising approach to ensure high-bandwidth and efficient transmission. Specifically, to accommodate a 10 Tbps network traffic demand in SCNs, a total of one hundred 32 Gbaud dual-polarization quadrature phase shift keying (DP-QPSK) optical carriers (OCs) would be required if we assume 7 Gbaud for error-correcting code (ECC). To support a 10 Tbps Nyquist-wavelength division multiplexing (N-WDM) spectral super-channel (SpCh), the total spectrum resources required is 3.2 THz in the ideal case, nearly utilizing the entire C-band. Given this, wavelength switching becomes unnecessary for each spatial lane (SL) when the full spectrum resource of the C-band is allocated to a single connection request.

3.1. Spatial lane and spatial channel

SCNs have been regarded as a promising development in OTN transmission technology. It divides the optical layer into two separate layers: SDM and WDM layers. In the WDM layer, spectral SpCh has been proposed as a high-capacity optical channel (OCh) in elastic optical networks (EONs) [10]. A spectral SpCh is formed by combining multiple adjacent subcarriers, making efficient use of a broad range of contiguous spectrum resources. In the SDM layer, an SDM link is composed of multiple SLs. Each SL can either be a single-mode fiber (SMF) in a bundle of parallel SMFs or a core in an MCF.

In SCNs, a spatial channel (SCh) is characterized as an ultrahigh-capacity optical data stream that occupies a significant portion of the available spectrum resource. As shown in Fig. 1, SCNs offer four distinct types of SChs based on the number of OChs they carry:

- Type I: A SCh carries a single OCh or spectral SpCh that occupies nearly the entire spectrum resource of the C-band. In this case, the SCh of Type I can be transmitted through optical bypass end-to-end, eliminating the need for wavelength switching. For example, if a request to be transmitted between node pair A and D requires 360 FSs, an SCh of Type I whose size is 320 FSs is served for the end-to-end transmission of a portion of this request.
- Type II: A SCh carries multiple OChs or spectral SpChs, all of which share the same source–destination pair. In this case, wavelength switching is also not required for routing the SCh of Type II. For example, an SCh of Type II is employed to enable end-to-end transmission of two requests with identical node pairs, where the combined requirement of FSs totals 320.
- Type III: A SCh carries multiple OChs or spectral SpChs that have different source–destination pairs. In this case, OChs can be added or dropped at the intermediate node using WXCs. Thus, switching GBs between different OChs are necessary. For example, after being served by an SCh of Type I, the remaining 40 FSs of the request between node pair A and D, along with a new incoming request from node B to C, need to be transmitted by an SCh of Type III with a GB between them. This is due to their different node pairs and small request sizes.
- Type IV: A SCh carries a single OCh or spectral SpCh of huge capacity that spans multiple SLs. The SCh of Type IV can be regarded as a special case of the SCh of Type I. Similar to Type I, wavelength switching is also not required for transmitting the SCh of Type IV. For example, an SCh of Type IV, which contains two SLs, is used to support the end-to-end transmission of a request requiring 640 FSs from node A to C.

3.2. Advantages and challenges of spatial channel networks

To address the challenge of achieving ultra-capacity transmission, there are two viable strategies: one is to scale up ROADMs or WXCs, and the other focuses on improving transmission efficiency instead of using high port-count ROADMs or WXCs. The first approach faces practical difficulties and is not cost-efficient due to the technical limitations of WSSs. SCNs introduce SXCs to facilitate two transmission modes, spatial bypass and wavelength switching, offering an alternative to expanding ROADMs or WXCs. Compared to traditional SDM networks, SCNs have the following advantages:

(1) Reduced insertion loss. As shown in Fig. 2, WSSs route various wavelength channels on the line side of the ROADM in SDM networks, whereas in SCNs, CSSs switch different spatial channels (fibers) on the line side of the HOXC. The usage of CSSs (7 dB) substantially lowers the insertion loss compared to WSSs (20 dB) [24].
(2) Extended transmission reach. Optical amplifiers (OAs) offset power loss caused by insertion loss but also add noise during amplification. A lower insertion loss reduces the introduction of noise, enhancing the Optical Signal to Noise Ratio (OSNR) and allowing for longer end-to-end transmission distances without regeneration points. Moreover, spatially bypassed optical signals can be transmitted further because they do not need to pass through the WXC.
(3) Reduced costs. The longer transmission reach enabled by CSS-based line sides reduces the number of required regeneration points for long-haul transmission, thereby lowering overall costs. Additionally, CSSs are more cost-effective than WSSs [25], further contributing to cost savings.
(4) Greater scalability. The free-space optics-based CSS offers easy scalability and reconfiguration, facilitating the expansion of mesh networks.

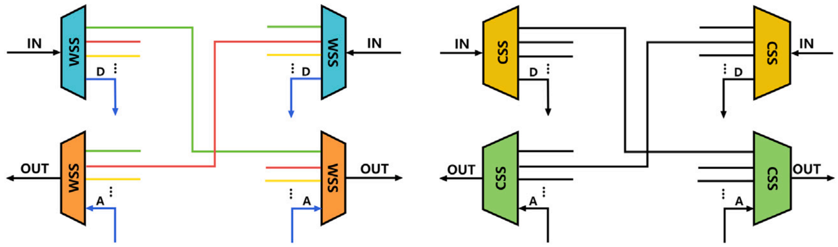

(a) The WSS-based line side. (b) The CSS-based line side.

Fig. 2. The WSS-based line side in a ROADM vs. the CSS-based line side in a HOXC.

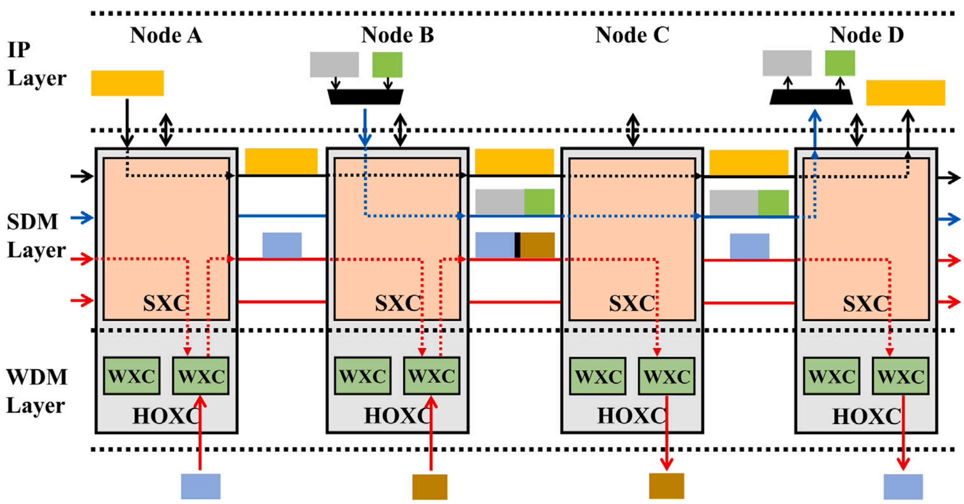

Fig. 3. Architecture of an SCN.

The hierarchical WDM and SDM layers of SCNs offer considerable benefits but also introduce challenges in designing optical node architecture. It is critical to emphasize that once the architecture of an optical node is established, the significant cost involved makes it challenging to change. Therefore, determining the optimal design for HOXC in SCNs to meet traffic demands remains a pivotal concern.

In a HOXC, the main and edge switches, known as the SXC and WXC, handle multiplexing and grooming at the SL and wavelength levels, respectively. SLs supported in an SXC fall into two categories: those subject to spatial bypass and those amenable to wavelength switching. The proportion of SLs capable of wavelength switching, which defines the wavelength switching granularity, plays a crucial role in determining the distribution of these two types of SLs. This granularity also influences the port count of the WXC, where a lower granularity enhances cost efficiency at the expense of routing flexibility, and vice versa for higher granularity. The selection of wavelength switching granularity is thus crucial for both node architecture design and the overall network evaluation in SCNs, forming the core focus of this study.

3.3. Architecture of an SCN and its components

The basic architecture of an SCN is designed to separate the optical layer into hierarchical SDM and WDM layers. As shown in Fig. 3, SChs of Type I, Type II, and Type IV are transmitted without the need for wavelength switching and bypass the WDM layer. Fig. 3 illustrates the physical implementation of independent spatial and wavelength switching by a HOXC, which consists of an SXC and multiple WXCs.

In an SCN, certain types of SChs can be especially beneficial for specific transmission requirements. For example, SChs of Type I and Type II are particularly useful when a single or aggregated optical data stream between a source–destination pair nearly fills the capacity of an entire SCh. These two types of SChs operate in the SDM layer and do not require wavelength switching, which leads to reduced switching costs and more efficient use of resources [2]. In addition, when multiple low-capacity OChs or spectral SpChs need to be transmitted between different source–destination pairs, they can be grouped into an SCh of Type III. These low-capacity channels can be added or dropped at intermediate nodes in the WDM layer using WXCs. While this increases spectrum usage due to the necessary GBs, it also improves the routing flexibility. As for the SCh of Type IV, they serve as an extension of Type I but are designed to accommodate OChs whose capacity surpasses that of a single SCh. To handle these high-capacity channels, multiple SLs within the SDM link are allocated. To support these diverse types of SChs, the HOXC architecture, consisting of an SXC and several WXCs, has been proposed and further developed [26–29].

Four different types of HOXCs have been proposed in [2] to provide a range of benefits, including routing flexibility, scalability, and cost efficiency in SCNs. These types are implemented based on different switch architectures, namely core-selective switch (CSS) [16] and matrix switch (MS) [30]. The four types are: full-size CSS-based HOXC, full-size MS-based HOXC, sub-CSS-based HOXC, and sub-MS-based HOXC. CSS-based HOXCs have been noted for their lower node costs compared to their MS-based counterparts [2,15]. Moreover, the higher complexity and integration level of the MS architecture pose challenges in supporting the scaling up of nodal degree and the number of SLs. Given these considerations, this paper will focus specifically on the architecture of CSS-based HOXCs, which appear to be a more practical choice for future commercial implementations of SCNs [20].

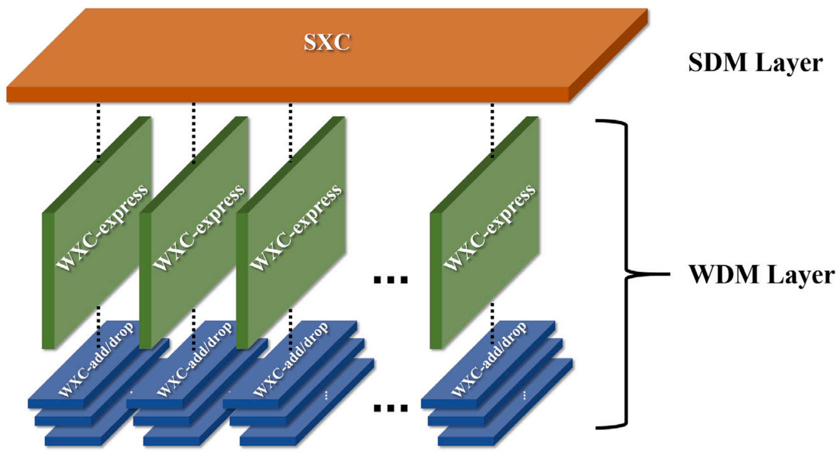

Fig. 4. SDM and WDM layers in a HOXC.

Table 2
Parameters used in this paper.

Para.	Meaning
C	The number of cores in a MCF
M	The number of WXCs per HOXC
K	The port number of a $K \times K$ WSS-based WXC
O	The number of add/drop ports supported by a WSS
N	The port number of a CSS
D	The node degree
T	The number of transceivers supported per WXC
V	The number of nodes in the network
h	The proportion of SLs supporting wavelength switching

3.4. Architecture of a HOXC and cost analysis

By leveraging a hierarchical structure, the HOXC efficiently manages both spatial and wavelength channels through separate components: the SXC and the WXC. The SXC serves as a key element of the HOXC, designed to deal with spatial channels. It enables the routing of optical signals across different SLs without requiring wavelength switching. On the other hand, the WXC is responsible for managing and switching optical signals at different wavelengths.

As shown in Fig. 4, the HOXC distinguishes SCNs from traditional SDM networks through its hierarchical design, consisting of an SDM layer and a WDM layer. In the SDM layer, the SXC enables part of the SLs to support spatial bypass transmission, while the remainder are directed to WXCs/ROADMs in the WDM layer for wavelength switching. The quantity of WXCs correlates with the number of SLs supporting wavelength switching in the SXC. Each WXC consists of an express module and an add/drop module, with the design of the latter depending on the required number of transceivers at each node (see Table 2).

Fig. 5 illustrates the architecture of a HOXC in 4-core MCF-based SCNs at a node with a degree of 3. The HOXC consists of a 4 × {1 × (M+2)} CSS-based SXC and M WSS-based WXCs. As shown in Fig. 5(a), the design of an SXC is determined by the input and output MCFs. A C × (1 × N) CSS connects an input C-core MCF and N output C-core MCFs for each direction. Notably, extra spatial multiplexers (SMUXs) and spatial demultiplexers (SDEMUXs) are necessary for an SXC when the input fibers are bundles of parallel SMFs [25]. The quantity of WXCs in a HOXC depends on the number of SLs in the SXC capable of wavelength switching. Furthermore, as depicted in Fig. 5(b), the design of each WXC is contingent upon the core count of the input MCF, the node degree, and the number of add/drop ports a WSS can support. Therefore, the overall cost of a HOXC can be estimated by summing the costs of an SXC, several WXCs, and other optical components.

Table 3
The main components and corresponding quoted price of a C×(1×N) CSS.

Component	Price (unit:USD)	Quantity	Total cost
Collimating lens	85	C·(N+2)	85 ·C·(N+2)
Focusing lens	128	C·(N+2)	128 ·C·(N+2)
MEMS mirror	969	C+N+1	969 ·(C+N+1)

Fig. 6 presents the design of a 1 × N CSS, which has one input and N output C-core MCFs. Optical signals traveling through the cores of the input MCF are spatially demultiplexed by a 1 × C SDEMUX. These demultiplexed signals are then routed through C sets of 1 × N switches. Finally, the signals exiting the 1 × N switches are spatially multiplexed by N units of C × 1 SMUX, and transmitted to N output MCFs. However, commercial CSS solutions that are both cost-efficient and compact are currently not available [25]. One feasible approach for implementing it involves the use of free-space optics [16,17].

The primary role of the CSS is to enable the routing of a light beam from any core of the input MCF to the corresponding core in any of the output MCFs. By employing free-space optics-based CSSs to implement the SXC, it can achieve a route-and-select (R&S) configuration. This setup enables the establishment of the connections between input and output cores with the same index. In a C × (1 × N) CSS, each of the C cores in the input MCF can be routed to any of the N output MCFs. As stated in [25], a CSS based on free-space optics comprises a 2D collimating lens array, a condenser lens, and an array of switching elements. Specifically, a single 1 × C SDEMUX is required, along with N units of C × 1 SMUXs. Furthermore, the CSS also needs C input collimating lenses for light collimation, C MEMS mirrors (including control modules) for beam steering, and C focusing lenses to concentrate the light [31,32]. Due to the lack of available commercial SMUXs and SDEMUXs, free-space optics can realize these functions by the use of lenses and mirrors. For a C × 1 SMUX or a 1 × C SDEMUX, C collimating lenses, one MEMS mirror, and C focusing lenses are needed. Table 3 lists the main components of a C × (1 × N) CSS and their corresponding quoted prices, based on information from the Edmund Optics [33] and eBay [34] website.

The cost of a C × (1 × N) CSS can be calculated based on the individual component costs and their respective quantities. Given that each component has a specific diameter according to [16]–2 mm for the collimating lens, 30 mm for the focusing lens, and 2 mm for the MEMS mirror–we can consult the information from Table 3 to arrive as the total cost:

$$\begin{aligned} C_{CSS} &= 85 \cdot C \cdot (N+2) + 128 \cdot C \cdot (N+2) + 969 \cdot (C+N+1) \\ &= 213 \cdot C \cdot (N+2) + 969 \cdot (C+N+1). \end{aligned} \tag{1}$$

To implement a CSS-based SXC at a node with a node degree of D, total 2D units of C × (1 × N) CSSs are required. The cost of a CSS-based

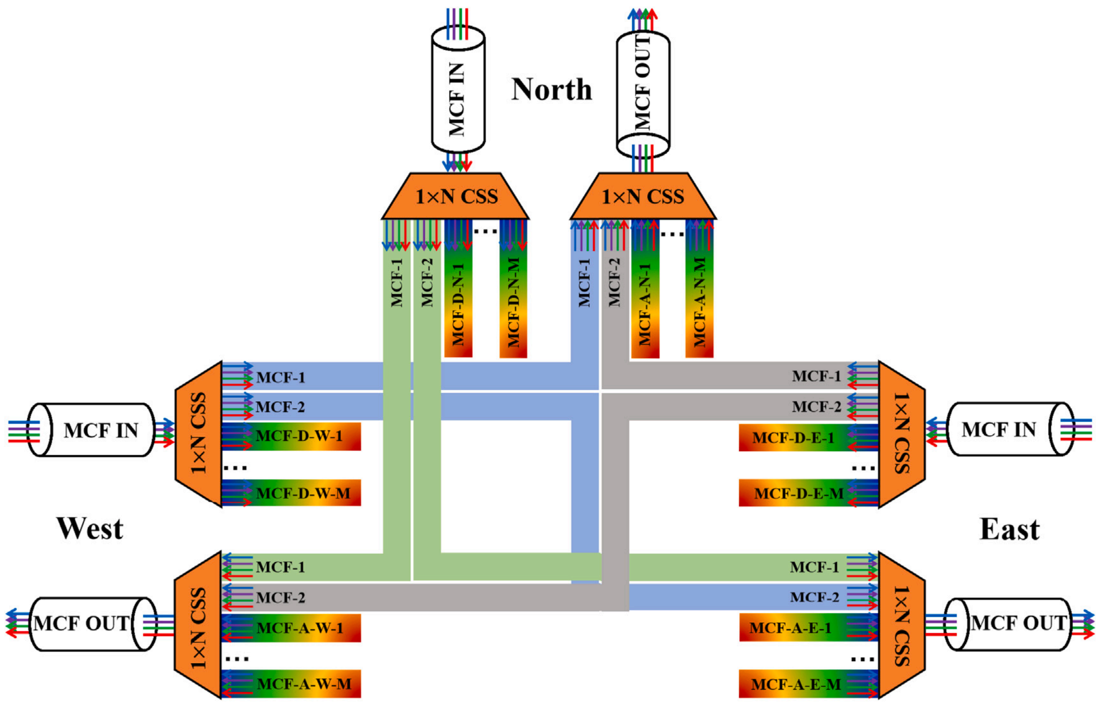

(a) Architecture of a 4×{1×(M+2)} CSS-based SXC.(N = M + 2)

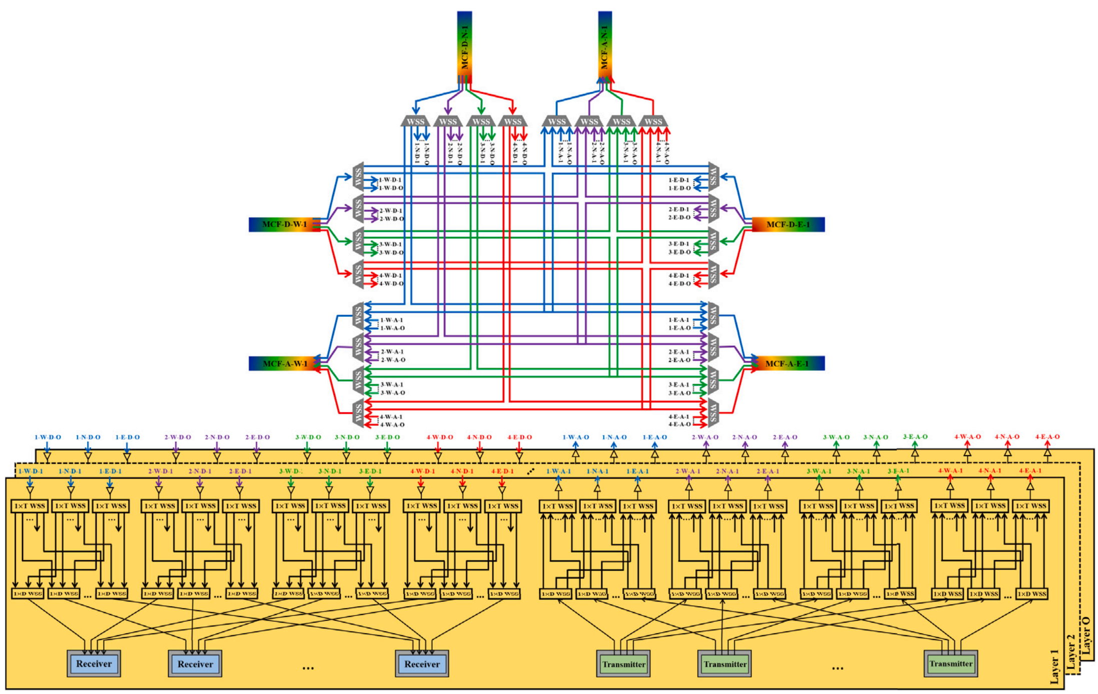

(b) Architecture of a WSS-based WXC: an express module and an add/drop module.

Fig. 5. Architecture of a HOXC in 4-core MCF-based SCNs for a node with a degree of 3.

SXC can be calculated by summing the costs of all the CSSs involved at this node.

$$C_{SXC} = \sum_{2D} C_{CSS} = 2 \cdot D \cdot \{213 \cdot C \cdot (N+2) + 969 \cdot (C+N+1)\}. \quad (2)$$

Another component of the HOXC is the WXC, which is used for wavelength switching. The WSS has been regarded as a key device for WXC nodes, as it can effectively reduce architecture complexity and insertion loss while enhancing scalability and flexibility [35–38].

The quantity of required WXCs depends on the number of SLs that support wavelength switching. Meanwhile, the port count of each WXC is determined by the core number of the MCF C, the number of deployed transceivers O, and the node degree D. The overall device cost of a WXC is closely related to its port count, which in turn is determined by the port number of the WSSs being used. Table 4 lists the quoted prices (unit: USD) for WSSs with different port counts [38–40].

For an input MCF with C cores processed through a C × (1 × N) CSS, N MCFs are output, each also having C cores. Out of these N output

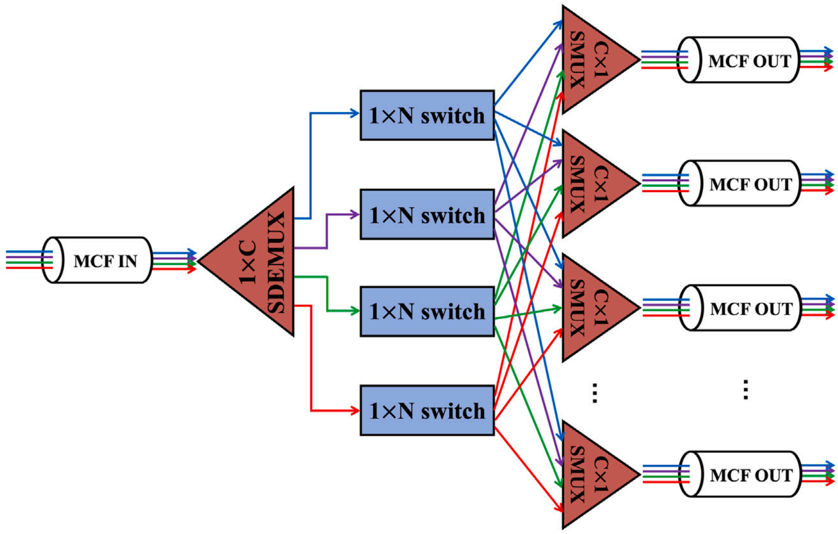

Fig. 6. Architecture of a C × (1 × N) CSS.

Table 4
The quoted prices of WSSs with different port counts.

WSS	1 × 40	1 × 20	1 × 9	1 × 5
C_{WSS}	25,500	16,200	10,200	6600

MCFs, at least D-1 output MCFs are used for direct switching via spatial bypass. If M of these output MCFs are set up to support wavelength switching, then to ensure both scalability and stability at each node, the total number of SLs in the output MCFs must exceed the combined sum of SLs in the MCFs that support wavelength switching and those used for spatial bypass.

$$C \cdot N \geq C \cdot M + C \cdot (D - 1). \tag{3}$$

In this case, the number of required WXCs, denoted by M, is obtained by rounding up the product of the proportion of SLs supporting wavelength switching and the total number of output MCFs. Given that each WXC accommodates T transceivers, the total number of transceivers deployed per node is $O = M \cdot T$. To accomplish a single WXC, 1 × T and 1 × D WSSs are employed, necessitating quantities of $2 \cdot D \cdot C$ and $2 \cdot T \cdot C$, respectively. Consequently, the cost of a WXC can be calculated as follows:

$$\begin{aligned} C_{WXC} &= \sum_{2D \cdot C} C_{1\times T\ WSS} + \sum_{2T \cdot C} C_{1\times D\ WSS} \\ &= 2 \cdot D \cdot C \cdot C_{1\times T\ WSS} + 2 \cdot T \cdot C \cdot C_{1\times D\ WSS}. \end{aligned} \tag{4}$$

In Fig. 5, the architecture of a HOXC features various essential components for all-optical transmission. Besides an SXC and multiple WXCs, the design incorporates specific optical elements. Notably, arrayed variable-gain dual-stage amplifiers (VGDAs) are included to amplify signals in both the input and output MCFs. Additionally, multiple SMUXs and SDEMUXs are utilized to establish connections between the add/drop ports of the SXC and the ports of the WXCs.

The cost of a VGDA is cited to be 5,400 USD [38]. The quantity of needed VGDAs for a node is determined by both the core number of MCFs and the node degree. Therefore, the total cost of the VGDAs required for an intermediate node with C cores in the input MCF and a node degree of D can be calculated as follows:

$$C_{VGDA} = 5,400 \cdot D \cdot C. \tag{5}$$

The cost of a C × 1 SMUX or a 1 × C SDEMUX is given by 213C + 969, and 2D units of SMUXs and SDEMUXs are needed for a single WXC. For a HOXC with M WXCs, the total cost of required SMUXs and SDEMUXs can be calculated using the following formula:

$$C_{SDEMUX+SMUX} = 2 \cdot D \cdot M \cdot (213 \cdot C + 969). \tag{6}$$

The overall cost of a HOXC employed at an intermediate node with a node degree of D, consisting of a C × (1 × N) CSS-based SXC and M WSS-based WXCs, can be calculated as follows:

$$\begin{aligned} C_{HOXC} =& C_{SXC} + M \cdot C_{WXC} + C_{VGDA} + C_{S(DE)MUX} \\ =& 2 \cdot D \cdot \{213 \cdot C \cdot (N+2) + 969 \cdot (C + N + 1)\} \\ &+ M \cdot \{2 \cdot D \cdot C \cdot C_{1\times T\ WSS} + 2 \cdot T \cdot C \cdot C_{1\times D\ WSS}\} \\ &+ 5,400 \cdot D \cdot C + 2 \cdot D \cdot M \cdot (213 \cdot C + 969). \end{aligned} \tag{7}$$

4. Adaptive dynamic RSCSA algorithm

We have developed an adaptive dynamic RSCSA algorithm to solve the routing and resource assignment problems in SCNs. The device cost and network performance metrics are measured after dynamically processing 10,000 requests, each arriving at a different time and having a varying duration. The arrival time for these requests begins at zero, with the interval between requests following an exponential distribution. Similarly, the duration of each request is also exponentially distributed.

To accommodate different wavelength switching granularities, we modify the holding time coefficient to change the duration of each request. This adjustment continues until the Bandwidth Blocking Probability (BBP) reaches 1%. Following this process, the final metrics used in this paper are derived by averaging the results of 50 different input request matrices. Each matrix maintains a consistent distribution of request sizes, ensuring a reliable assessment of our algorithm's effectiveness.

As illustrated in Fig. 7, our proposed RSCSA algorithm aims to allocate different types of SChs adaptively based on request size, thereby improving the utilization of channel spectrum resources and network throughput. In detail, we allocate the shortest path for each request between its source–destination pair. The SCh assignment for each request is determined using first fit (FF) and greedy strategies, with a focus on maximizing the utilization of various types of SChs. In addition, spectrum resource assignment is conducted using the best fit (BF) algorithm [41]. The main steps for processing a single request by our dynamic RSCSA algorithm can be summarized as follows:

(1) For each request $r(s_r, d_r, t_r)$ arriving at the network, compute the shortest path from source node s_r to destination node d_r.

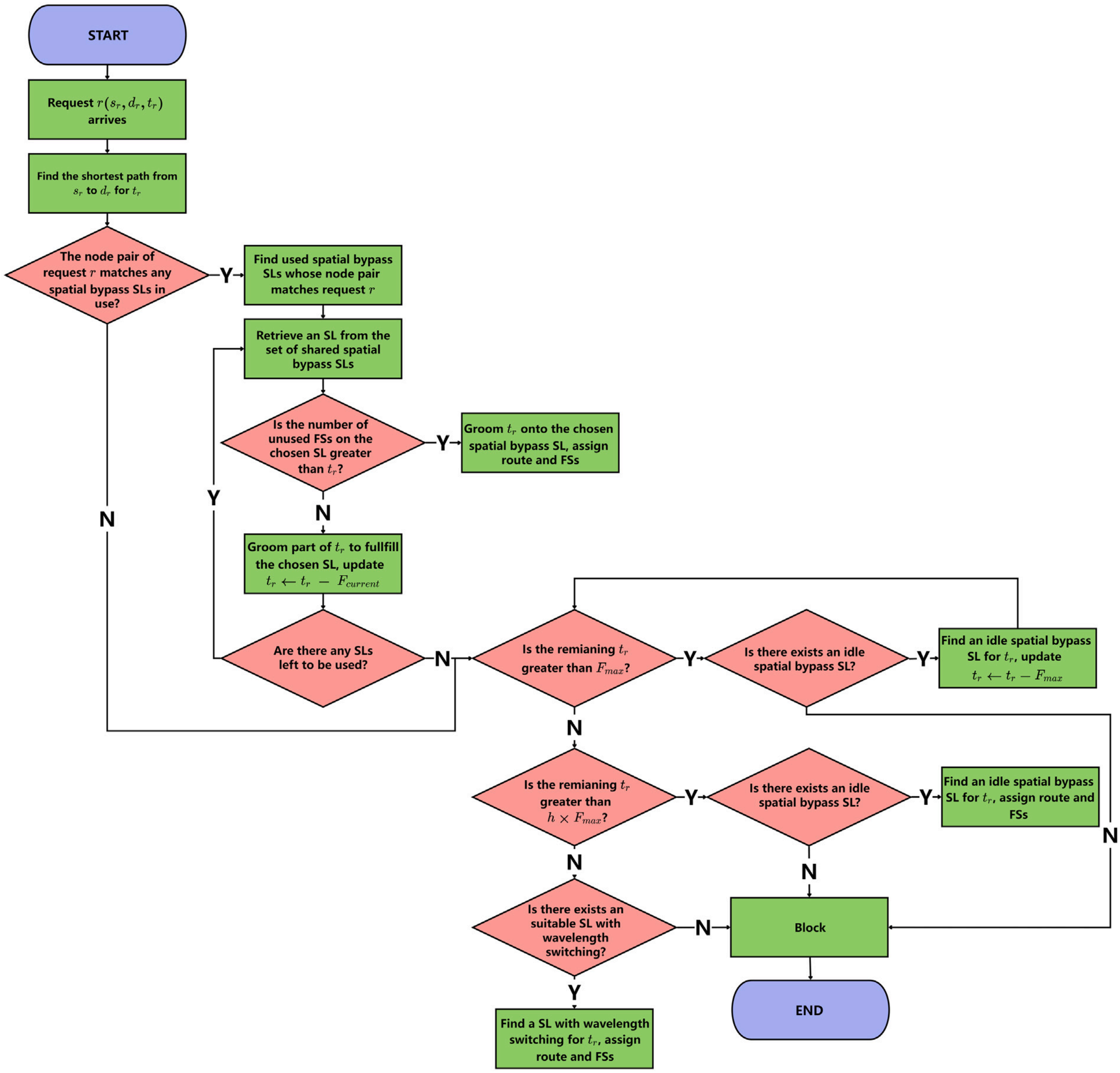

Fig. 7. Adaptive dynamic RSCSA algorithm.

(2) If the node pair of the spatial bypass SLs in use matches that of request r, proceed to step (3); otherwise, skip to step (8).
(3) Compile a set of the spatial bypass SLs in use whose node pair is s_r and d_r.
(4) Retrieve one from the set of shared spatial bypass SLs.
(5) If the number of unused FSs on the selected spatial bypass SL exceeds the FSs required for request r (t_r), groom t_r onto this SL, assign route and FSs to request r; if not, proceed to step 6.
(6) Allocate the unused FSs on the selected spatial bypass SL ($F_{current}$) to support part of t_r, and update $t_r \leftarrow t_r - F_{current}$.
(7) If there are unprocessed SLs in the set, return to step (4); if not, proceed to step (8).
(8) If t_r exceeds the total FSs in the C-band (F_{max}), proceed to step (9); if not, go to step (10).
(9) If an idle spatial bypass SL is available, allocate all FSs on it to support part of t_r and update $t_r \leftarrow t_r - F_{max}$, then return to step (8); if not available, block request r.
(10) If t_r is greater than the threshold $h \times F_{max}$, proceed to step (11); otherwise, go to step (12).
(11) If an idle spatial bypass SL is available, allocate FSs on it to support t_r, assign route and FSs to request r; If not, block request r.
(12) If there is an SL with wavelength switching having sufficient FSs for t_r, allocate these FSs to request t_r, assign route and FSs to request r; if not, block request r.

5. Network models and assumptions

5.1. Network model

In this section, we conduct simulations to evaluate the device cost, network throughput, and resource utilization of SCN transmission systems across different HOXC architectures. These simulations are performed in two network typologies shown in Fig. 8: the European Backbone Network (EBN) with 28 nodes and 68 directed links [39,40], and the American ATT Backbone Network (AABN) with 27 nodes and 74 directed links [40,41].

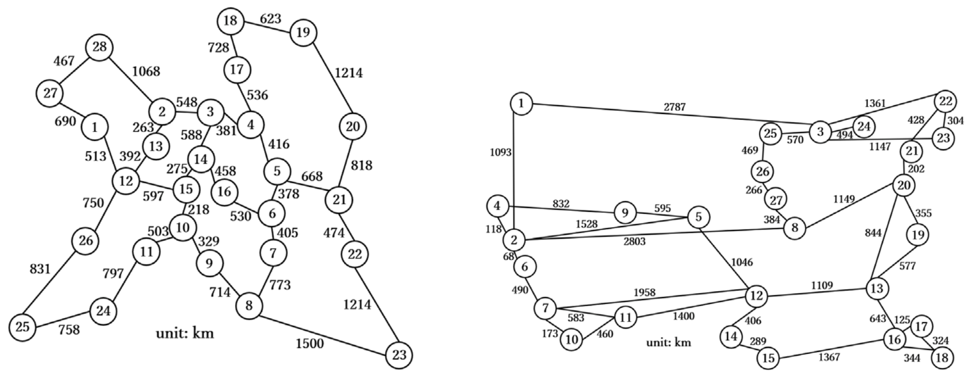

(a) European Backbone Network (EBN).

(b) American ATT Backbone Network (AABN).

Fig. 8. Network topology: (a) EBN; (b) AABN.

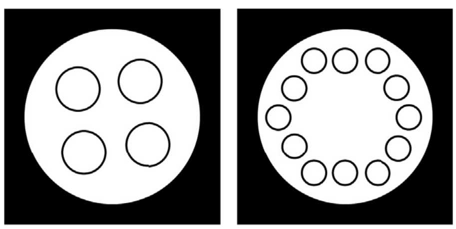

(a) A 4-core MCF (b) A 12-core MCF

Fig. 9. Examples of a 4-core MCF and a 12-core MCF.

Table 5
Physical features of a 4-core MCF and a 12-core MCF.

Fiber type	Λ [m]	k	β [1/m]	r [m]
4-core MCF	3.9×10^{-5} [42]	5×10^{-4}	4×10^{6}	5×10^{-2}
12-core MCF	3.7×10^{-5} [43]	1.4×10^{-3}	4×10^{6}	5×10^{-2}

5.2. Assumptions

The assumptions stated in the simulation experiments are as follows:

(1) The input MCFs used in this paper are 4-core MCFs and 12-core MCFs. Therefore, the link in our simulated network model is assumed to be a 4-core MCF-based link or a 12-core MCF-based link. The examples of a 4-core MCF and a 12-core MCF are shown in Fig. 9.
The physical features of a 4-core MCF and a 12-core MCF are illustrated in Table 5. Λ represents the core pitch, k is the coupling coefficient computed by Eq. (8),

$$k = 315530 \cdot e^{-0.519\Lambda}, \tag{8}$$

β and r are constant for different types of MCFs, which denote propagation constant and bending radius, respectively.

(2) The crosstalk (XT) is generated when signals are transmitted through adjacent cores at the same wavelength within MCFs. As indicated in [44,45], the physical characteristics of MCFs have an impact on XT. The XT of an MCF over L meters (unit: m) can be calculated as follows:

$$XT(L) = \frac{n - n \cdot exp\{-(n+1)2hL\}}{1 + n \cdot exp\{-(n+1)2hL\}}, \tag{9}$$

where n represents the number of adjacent cores, L is the transmission distance, and h = $\frac{2k^2 r}{\beta\Lambda}$ is a parameter that is related to the physical properties of MCFs. Assuming −16, −20.5, −23, −27, and −29 dB XT thresholds (with a −2 dB XT margin) for DP-BPSK, DP-QPSK, DP-8QAM, DP-16QAM, and DP-32QAM, the transmission reaches for different types of MCFs under various modulation formats, constrained by the optical signal-to-noise ratio (OSNR) or XT, can be computed using Eq. (9). These transmission reaches are summarized in Table 6.

Table 6
Transmission reaches for 4-core MCFs and 12-core MCFs.

Limitation factor	Transmission reach [km]				
	BPSK	QPSK	8QAM	16QAM	32QAM
OSNR	6300	3500	1200	600	268
XT in 4-core MCFs	38 945	13 872	7808	3111	1963
XT in 12-core MCFs	4712	1678	944	376	237

(3) In a 4-core MCF-based SCN, $4 \times (1 \times 9)$ CSSs are utilized for the HOXC. Similarly, for a 12-core MCF-based SCN, $12 \times (1 \times 9)$ CSSs is employed. The proportion of SLs that can support wavelength switching, compared to the total number of SLs, is assumed to range from 0.1 to 0.9, in increments of 0.1. The number of flexible 800G single-carrier transceivers deployed in each WXC is 16.

(4) The total available spectrum resource in each core of MCFs in this paper is 4 THz. According to ITU-T G.694.1, the 4 THz spectrum resource can be divided into 320 FSs, each of which occupies 12.5 GHz. An optical carrier (OC) is composed of three FSs, occupying 37.5 GHz of the spectrum resources. Furthermore, the switching GBs located on both sides of the OC totally occupy 6.25 GHz of the spectrum. Moreover, we assume that an OC can support 50 Gbps traffic under DP-BPSK.

(5) The number of requests in our simulation experiments is 10,000, and the request sizes are probabilistically generated to be 10 Tbps, 4 Tbps, 1 Tbps or 0.8 Tbps, with respective probabilities of 0.1, 0.1, 0.4, and 0.4. The requests, each associated with a specific source–destination pair, are expected to arrive at each network node following a Poisson process. This process is characterized by predefined average holding and arrival times. Furthermore, both the arrival and holding times adhere to a negative exponential distribution.

(6) The routing path of each request is the shortest path between its source–destination (sd) pair. The assignment of SCh and spectrum follows our proposed adaptive dynamic RSCSA algorithm, where the parameter h is set to 0.4 [3].

6. Performance metrics and results

In this paper, we use three key metrics of device cost, network throughput, and resource utilization for evaluating HOXC architectures

Table 7
The main components involved in the device cost.

Component	Quantity	Total cost
HOXC	V	V $\cdot$ C_{HOXC}
Transceiver	V $\cdot$ O	V $\cdot$ O $\cdot$ C_{TRAN}

with different wavelength switching granularities [46,47]. The final results of these metrics are obtained by adjusting the holding time coefficient of requests, which represents the average duration of all requests in the network, until the bandwidth blocking probability (BBP) of 10,000 requests reaches a reasonable 1%.

In this section, we offer a thorough breakdown of each metric and give a detailed analysis of the corresponding result. For different proportions of SLs supporting wavelength switching, we investigate the architecture of the HOXC, which encompasses both the SXC and the WXCs, at each node in EBN and AABN. To guarantee generality, our findings are obtained by taking the average over 50 simulation runs with the inputs of independently and randomly generated traffic matrices. In addition, to maintain fairness, all the input request matrices have the same request size distribution.

6.1. Device cost

The device cost in optical networks is defined as the cumulative expense of various components, with particular emphasis on ROADMs and transceivers. These are the two most significant cost-driving elements in the system. In this paper, our measure of device cost is the total cost of all HOXCs and transceivers deployed on the entire network topology.

According to the findings in [38], the cost of a 100G DP-QPSK single-carrier transceiver is reported to be 30,000 USD. When transitioning to an integrated super-channel (SpCh) transceiver that supports eight sub-channels in a Nyquist WDM (NWDM) configuration, the per sub-channel cost is expected to be decreased by 23%. Furthermore, the standard coherent DP-QPSK transceiver can be implemented into a reconfigurable coherent transceiver without the need for changing the architecture [48]. With these considerations in mind, the cost of a flexible 800G single-carrier transceiver capable of supporting variable modulation formats can be calculated as follows:

$$C_{TRAN} = 30,000 \cdot 8 \cdot 0.77 = 184,800. \tag{10}$$

The count of transceivers at each node is determined by the number of WXCs deployed per HOXC, with each WXC equipped with T transceivers. This requirement for WXCs depends on both the core number of MCFs and the proportion of SLs supporting wavelength switching. With a pre-defined proportion of SLs supporting wavelength switching h, we have the number of WXCs per HOXC:

$$M = \lceil h \cdot (C \cdot N) \rceil. \tag{11}$$

Therefore, we can obtain the total number of transceivers per node as follows:

$$O = T \cdot M. \tag{12}$$

The overall device cost, denoted as DC, can be computed by summing the costs of deployed HOXCs and transceivers at all the network nodes:

$$DC = V \cdot O \cdot C_{TRAN} + V \cdot C_{HOXC}. \tag{13}$$

According to the cost of a HOXC and a transceiver mentioned in Eqs. (7) and (13), respectively, the device cost is related to several factors. These include the number of required WXCs, denoted by M; the total number of network nodes, denoted by V; the number of transceivers installed at each node, denoted by O; the number of output MCFs supported by CSSs, denoted by N; and the core number of MCFs, denoted by C (see Table 7).

In this paper, each WXC is assumed to support 16 transceivers, denoted as $T = 16$. In systems utilizing 4-core and 12-core MCFs, the requirement for transceivers increases proportionally with the number of SLs capable of wavelength switching. When the proportion of SLs supporting wavelength h remains constant, the total cost of transceivers in a network is directly related to the total number of network nodes and SLs. Therefore, systems based on 12-core MCFs incur higher transceiver costs compared to those using 4-core MCFs. Similarly, the cost of transceivers in AABN surpasses that in EBN.

Fig. 10 shows the device costs (unit: billion USD) varying with the proportion of SLs supporting wavelength switching in different network topologies and input MCFs. As indicated in Fig. 10(a), for both 4-core MCF-based EBN and AABN, there is a noticeable rising trend in device costs as the proportion of SLs supporting wavelength switching increases. This rise in device cost is primarily driven by the cost of HOXCs, which is, in turn, determined by the number of required WXCs–directly influenced by the proportion of SLs supporting wavelength switching. Note that the number of transceivers employed in each WXC is fixed, the device costs of both EBN and AABN are roughly identical in the same proportion, with slightly more in EBN due to its larger number of network nodes and average node degree. Fig. 10(b) presents the relationship between device costs and the proportion of SLs supporting wavelength switching in a 12-core MCF-based EBN and AABN. The trend of its curves in different topologies is similar to that of using 4-core MCFs.

With the comparison between Figs. 10(a) and 10(b), it is clear that while both state similar overall trends, the curve in Fig. 10(b) has a steeper slope when using 12-core MCFs. This implies that the device costs of 12-core MCF-based networks escalate more sharply as the proportion of SLs supporting wavelength switching increases. Such differences between the two figures highlight the significant role that the number of cores plays in influencing the total device cost.

As depicted in Fig. 11, the device cost of a 12-core MCF-based EBN is about 12 to 24 times higher than that of a 4-core MCF-based EBN with the increasing proportion of SLs supporting wavelength switching. With 12-core MCFs, the number of available spatial channels reaches 108, significantly surpassing the 36 available spatial channels with 4-core MCFs. Consequently, when adjusting the ratio of wavelength switching, the 12-core fiber optic system supports a much greater number of channels dedicated to wavelength switching compared to the 4-core system. The quantity of wavelength switching channels supported is the primary factor influencing equipment costs, leading to a more significant cost increase for the 12-core system than for the 4-core system.

For network operators deploying SCNs, opting for a lower proportion of SLs supporting wavelength switching might appear to be a cost-effective choice if device cost is the sole consideration. However, this narrow focus on device cost alone is inadequate for effective network planning. A balanced approach, which considers not only the device cost but also key performance metrics such as network throughput and resource utilization, is imperative for achieving both cost efficiency and good performance.

6.2. Network throughput

Network throughput refers to the rate at which data is successfully transmitted over a network, serving as a measure of network data processing efficiency [49]. In this paper, the network throughput is defined as the highest rate at which traffic data can be transmitted over the network, averaged over a certain period of time. As demonstrated in Eq. (14), network throughput (NT) (unit: Tbps) is calculated as the total amount of successfully transmitted traffic data divided by the total simulation duration, with a reasonable BBP [50].

$$NT = \frac{\sum_i tr_i \cdot t_i}{T_s}, \tag{14}$$

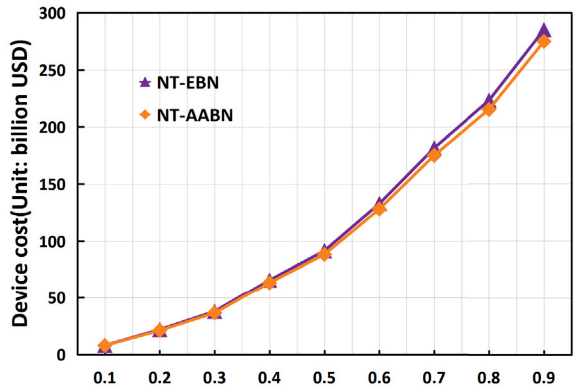

(a) In the context of a 4-core MCF-based EBN and AABN.

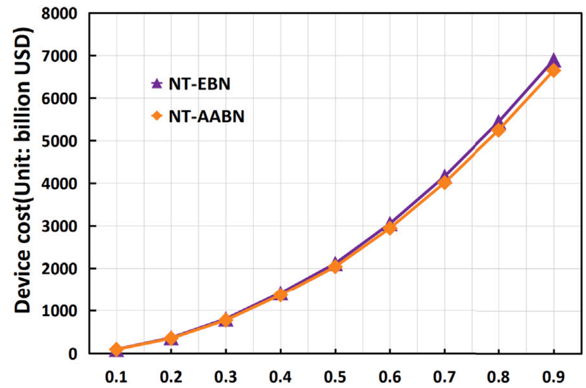

(b) In the context of a 12-core MCF-based EBN and AABN.

Fig. 10. Device cost vs. Proportions of SLs supporting wavelength switching in different network topologies and input MCFs: (a) in a 4-core MCF-based EBN and AABN; (b) in a 12-core MCF-based EBN and AABN.

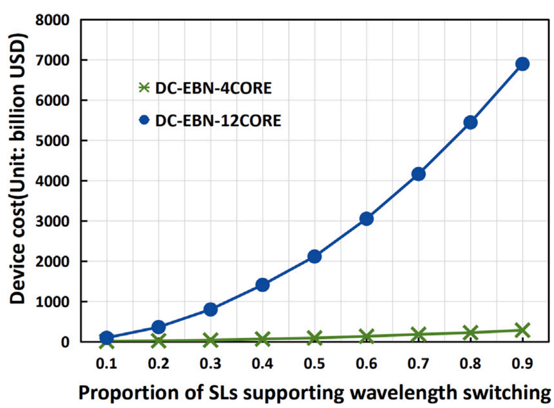

Fig. 11. Comparison of device costs in a 4-core and a 12-core MCF-based EBN.

where i represents the index of a successfully processed request, tr_i denotes the size of the ith request (unit: Tbps), t_i is the duration of the ith request, and T_s is the total duration of the simulation.

Fig. 12 depicts how network throughput (measured in Tbps) varies with the proportion of SLs that support wavelength switching in different transmission systems. As illustrated in Figs. 12(a) and 12(b), the network throughput of a 4-core MCF-based EBN consistently surpasses that of its AABN counterpart, regardless of the proportion of SLs supporting wavelength switching. The average link length in EBN is 629.9 km, which is shorter than the 786.2 km average in AABN. Moreover, the maximum link lengths in EBN and AABN are 1500 km and 2803 km, respectively. This reduction in average transmission distance, coupled with a more concentrated distribution of network nodes in EBN, allows for the utilization of higher modulation formats, thereby reducing the number of required OCs. Therefore, a given spectrum resource in EBN can accommodate more transmission requests, leading to an increase in overall network throughput.

In Figs. 12(a) and 12(b), the trends depicting the variation in network throughput with the proportion of SLs supporting wavelength switching are similar, showing initially a positive and then a negative correlation between them. The convex nature of the curves in both figures suggests that it is possible to identify the proportion of SLs supporting wavelength switching for optimal network throughput.

In SCNs, SLs that support wavelength switching are typically used for transmitting small requests, while SLs with spatial bypass are used for large requests. When the proportion of SLs supporting wavelength switching initially increases, the number of SLs capable of wavelength switching also increases. This improves routing flexibility, allowing more requests to be served in the network and thereby increasing network throughput. However, if the proportion continues to increase, the number of SLs with wavelength switching may exceed those with spatial bypass. In this case, network throughput decreases for two main reasons: (1) increased usage of SLs supporting wavelength switching leads to more guard bands (GBs), reducing spectrum utilization; (2) more large requests are blocked due to the insufficient number of SLs with spatial bypass.

In Fig. 12(a), for networks based on 4-core MCFs, the ideal proportions of SLs supporting wavelength switching are found to be 0.4 for EBN and 0.3 for AABN. Similarly, in 12-core MCF-based systems, the optimal proportions are 0.3 for EBN and 0.2 for AABN. Lower proportions of SLs supporting wavelength switching result in reduced routing flexibility, as most SLs are spatially bypassed, while higher proportions cause increased spectrum usage for GBs as most SLs support wavelength switching. Therefore, network throughput does not perform well in both scenarios. Overall, when focusing solely on maximizing network throughput for network planning, the recommended proportions of SLs supporting wavelength switching are 0.4 and 0.3 for 4-core and 12-core MCF-based EBNs, respectively, and 0.3 and 0.2 for 4-core and 12-core MCF-based AABNs, respectively.

6.3. Resource utilization

Resource utilization denotes the proportion of utilized network capacity relative to the total capacity available. In this paper, resource utilization (RU) is computed as the ratio of the total spectrum resources consumed for data transmission to the total available spectrum resources.

$$RU = \frac{\sum_i f_i}{\sum_i (f_i + f_i^{sw})} \cdot 100\%, \tag{15}$$

where f_i represents the spectrum resources consumed for the transmission of the ith request, and f_i^{sw} is the spectrum resources utilized as switching GBs for the transmission of the ith request.

Fig. 13 shows the resource utilization (unit: %) against different optical transmission systems. On the whole, as the proportion of SLs supporting wavelength switching rises from 0.1 to 1.0, the increasing capability for wavelength switching enhances routing flexibility but also results in greater GBs, leading to a decrease in resource utilization.

Figs. 13(a) and 13(b) present the variations in resource utilization under 4-core MCF-based and 12-core MCF-based optical networks,

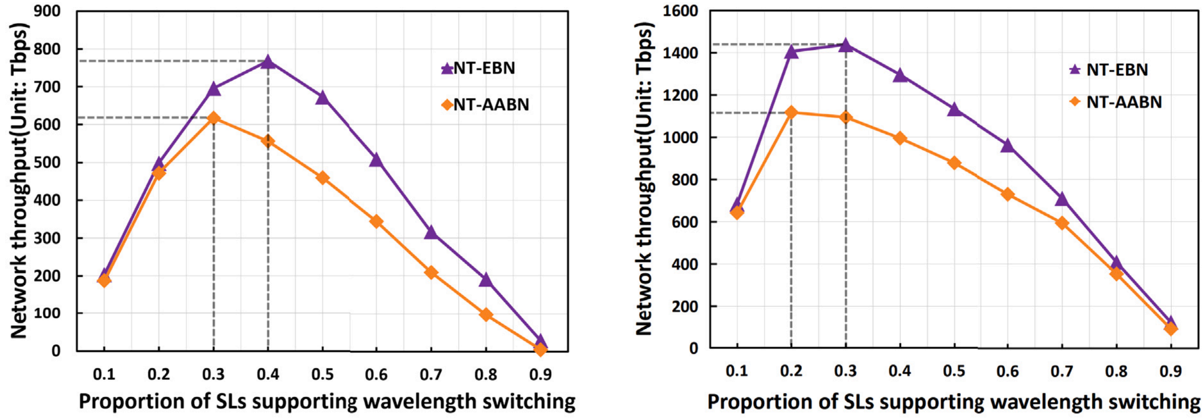

(a) In the context of a 4-core MCF-based EBN and AABN.

(b) In the context of a 12-core MCF-based EBN and AABN.

Fig. 12. Network throughput vs. Proportions of SLs supporting wavelength switching in different network topologies and input MCFs: (a) in a 4-core MCF-based EBN and AABN; (b) in a 12-core MCF-based EBN and AABN.

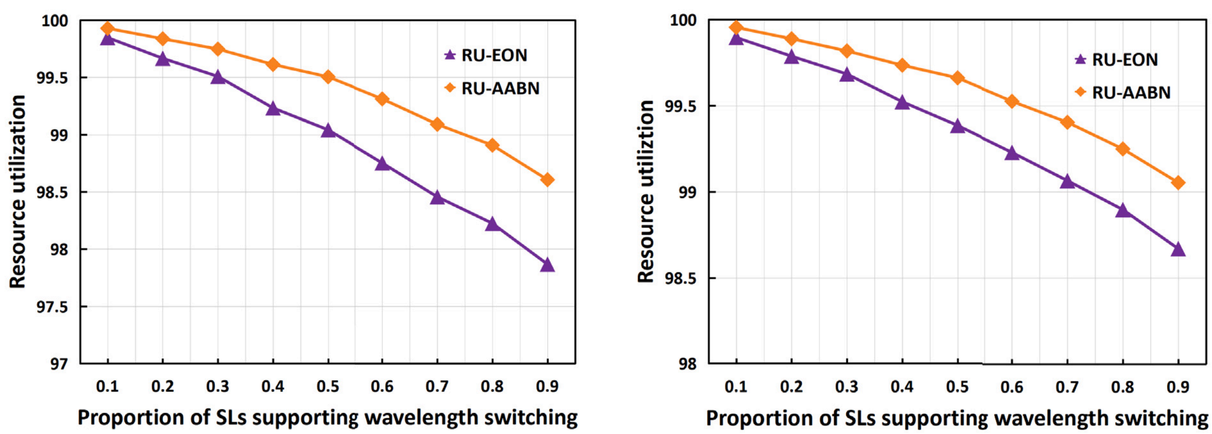

(a) In the context of a 4-core MCF-based EBN and AABN.

(b) In the context of a 12-core MCF-based EBN and AABN.

Fig. 13. Resource utilization vs. Proportions of SLs supporting wavelength switching in different network topologies and input MCFs: (a) in a 4-core MCF-based EBN and AABN; (b) in a 12-core MCF-based EBN and AABN.

respectively. Regardless of the network topology and the type of input MCF used, a negative correlation exists between resource utilization and the proportion of SLs supporting wavelength switching. As the proportion increases, so does the number of employed WXCs. This reduces the number of requests to be transmitted via optical bypass in an end-to-end manner through SXC. Therefore, more requests are transmitted across the SLs supporting wavelength switching, thereby necessitating more extra spectrum resources for GBs and ultimately resulting in lower resource utilization.

As shown in Figs. 13(a) and 13(b), the resource utilization in AABN consistently outperforms that in EBN under the same conditions. Notably, the gap in resource utilization between the two networks widens as the proportion of SLs supporting wavelength switching increases. As mentioned before, the shorter average link distance in EBN results in shorter routing paths for requests, enabling the use of higher-level modulation formats. Consequently, given the same available spectrum resources, EBN can accommodate more adjacent SChs but necessitates more additional GBs for their separation. This effect becomes increasingly pronounced as the proportion of SLs supporting wavelength switching grows, leading to generally lower resource utilization in EBN compared to AABN, along with an expanding gap between the two.

6.4. *Results of the trade-off between device cost and network throughput*

A trade-off exists among different network performance metrics, including device cost, network throughput, and resource utilization. Specifically, device cost and network throughput exhibit opposite trends compared to resource utilization, as the proportion of SLs supporting wavelength switching changes. Focusing on different performance indicators, the optimal proportion of SLs with wavelength switching capabilities can be determined, leading to the most efficient architecture of HOXC for different SCN-based transmission systems. Due to significant differences in the order of magnitude across these performance metrics, normalization is essential for meaningful comparison. We employ the min–max scaling method to ensure comparability between these different metrics, whose equation is shown as follows:

$$x_{nom} = \frac{x - x_{min}}{x_{max} - x_{min}}. \quad (16)$$

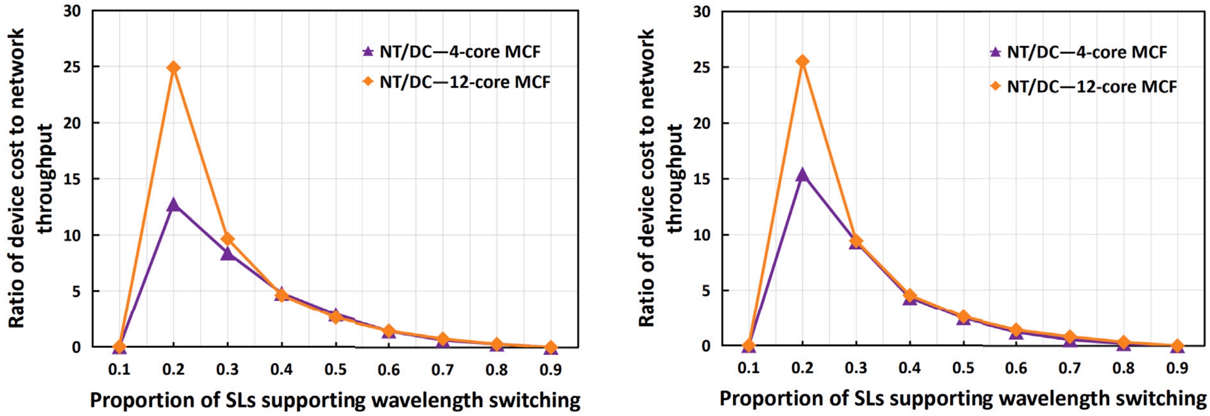

(a) In the context of EBN.

(b) In the context of AABN.

Fig. 14. Ratio of device cost to network throughput vs. Proportions of SLs supporting wavelength switching in different network topologies and input MCFs: (a) in 4-core and 12-core MCF-based EBNs; (b) in 4-core and 12-core MCF-based AABNs.

A transmission system that features low device cost, high network throughput, and high resource utilization is considered well-behaved. Given the strong performance in resource utilization we observed in both 4-core and 12-core MCF-based transmission systems ($\geq$ 97.6%), our analysis primarily focuses on the trade-off between device cost and network throughput, which are the two most critical factors considered in real-world commercial network operations.

Following normalization using the min–max scaling method, we introduce the ratio approach to solve this multi-objective problem and identify the optimal HOXC architectures for various transmission systems. As shown in Eq. (17), we employ the ratio of device cost to network throughput as a metric to quantify the amount of throughput per unit of device cost in different systems.

The ratio of device cost to network performance, denoted by J, serves as an effective metric to balance the trade-off between these two aspects. This is due to their interchangeability and non-linear relationship between them. As demonstrated by the correlation and regression analysis, the Pearson correlation coefficient between device cost and network throughput is 0.994, signaling a very strong positive correlation. Furthermore, the value of R^2 in the linear regression model stands at 0.987, indicating a well-fitting model where approximately 98.7% of the variation in network throughput variation can be attributed to device cost. Therefore, the results presented in Fig. 14 offer a reliable insight into the trade-off between device cost and network throughput.

$$J = \frac{network\ throughput}{device\ cost}. \tag{17}$$

When a higher value of Eq. (17) is considered as an indicator of better performance, a proportion of 0.1 for SLs supporting wavelength switching is not optimal. At this proportion, both the device cost and network throughput are minimized. Therefore, the value of Eq. (17) corresponding to a proportion of 0.1 is set as the lower bound. As the proportion of SLs supporting wavelength switching increases from 0.2 to 0.9, different transmission systems can yield optimal solutions to achieve the largest ratio of device cost to network throughput.

Specifically, Fig. 14(a) illustrates how the ratio in EBN changes with varying proportions of SLs supporting wavelength switching. In 4-core and 12-core MCF-based EBNs, a proportion of 0.2 emerges as the most balanced choice, considering both device cost and network throughput. Similarly, a proportion of 0.2 also performs well in AABNs. Moreover, in 12-core MCF-based systems, a proportion of 0.2 yields a more significant improvement in the ratio of device cost to network performance compared to 4-core MCF-based systems. This is attributed to the fact that in a 12-core MCF-based system(with a total of 108 SLs), an increase of 0.1 in the proportion of SLs supporting wavelength switching results in nearly 10 additional WXC layers, significantly increasing the device cost and thereby becoming the dominant factor in the ratio. In addition, network throughputs perform well at a proportion of 0.2 in all four different systems(although not optimal). Given the limited number of available SLs in 4-core MCF-based systems, an increase in the proportion of SLs supporting wavelength switching leads to a relatively smaller rise in device cost. This results in the curves of 4-core MCF-based systems not so steep as those of 12-core MCF-based systems.

7. Conclusions

In this paper, we present a comprehensive analysis of the deployment costs and network performance of SCNs, taking into account HOXC architectures with varying wavelength switching granularities and input MCFs. Detailed models are introduced to quantify key performance metrics, including device cost, network throughput, and resource utilization. To assess the efficiency of different SCN architectures, we conduct simulation experiments to solve dynamic RSCSA problems using our proposed adaptive dynamic RSCSA algorithm. Our experiment results, drawn from 4-core and 12-core MCF-based EBNs and AABNs, demonstrate that the architecture of HOXC–characterized by the proportion of SLs supporting wavelength switching in this paper–significantly impacts device cost, network throughput, and resource utilization. Specifically, device cost positively correlates with this proportion, while resource utilization shows an inverse relationship. Network throughput initially increases with the proportion but subsequently decreases. Notably, the high resource utilization observed across all transmission systems tested affirms the hierarchical optical layer's enhanced efficiency in SCNs for resource allocation. Furthermore, when considering the trade-off between device cost and network throughput, the proportion of 0.2 emerges as an optimal choice for four transmission systems. The metrics prioritized by network operators will influence these optimal proportions. For future research, we aim to simultaneously investigate the impact of changes in wavelength switching granularity and add/drop rate on assessing the device cost and network performance of SCNs. Furthermore, we intend to develop a reinforcement learning model to determine the optimal wavelength switching granularity across various request distributions, thus mitigating excessive computation time during dynamic experiments.

Declaration of competing interest

The authors declare the following financial interests/personal relationships which may be considered as potential competing interests: Yongbing Zhang reports financial support was provided by Japan Society for the Promotion of Science. Weichang Zheng reports financial support was provided by Quzhou Municipal Government. If there are other authors, they declare that they have no known competing financial interests or personal relationships that could have appeared to influence the work reported in this paper.

Data availability

Data will be made available on request.

Acknowledgments

This work has been partially supported by JSPS, Japan Grant -in-Aid for Scientific Research (C) 21K04544 and the Municipal Government of Quzhou, China No. 2023D028 and No. 2022D041.

References

[1] P.J. Winzer, D.T. Neilson, From scaling disparities to integrated parallelism: A decathlon for a decade, J. Lightwave Technol. 35 (5) (2017) 1099–1115.
[2] M. Jinno, Spatial channel network (SCN): opportunities and challenges of introducing spatial bypass toward the massive SDM era, J. Opt. Commun. Netw. 11 (3) (2019) 1–14.
[3] M. Jinno, Y. Asano, Y. Azuma, T. Kodama, R. Nakai, Technoeconomic analysis of spatial channel networks (SCNs): Benefits from spatial bypass and spectral grooming, J. Opt. Commun. Netw. 13 (2) (2021) A124–A134.
[4] B. Mukherjee, WDM optical communication networks: progress and challenges, IEEE J. Sel. Areas Commun. 18 (10) (2000) 1810–1824.
[5] K. Asatani, K.R. Harrison, R. Ballart, CCITT standardization of network node interface of synchronous digital hierarchy, IEEE Commun. Mag. 28 (8) (1990) 15–20.
[6] E. Modiano, A. Narula-Tam, Mechanisms for providing optical bypass in WDM-based networks, Opt. Netw. Mag. 1 (1) (2000) 11–18.
[7] M. Jinno, T. Kodama, T. Ishikawa, Feasibility demonstration of spatial channel networking using SDM/WDM hierarchical approach for peta-b/s optical transport, J. Lightw. Technol. 38 (9) (2020) 2577–2586.
[8] K. Zhu, B. Mukherjee, Traffic grooming in an optical WDM mesh network, IEEE J. Sel. Areas Commun. 20 (1) (2002) 122–133.
[9] S. Zhang, C. Martel, B. Mukherjee, Dynamic traffic grooming in elastic optical networks, IEEE J. Sel. Areas Commun. 31 (1) (2012) 4–12.
[10] M. Jinno, H. Takara, B. Kozicki, Y. Tsukishima, Y. Sone, S. Matsuoka, Spectrum-efficient and scalable elastic optical path network: architecture, benefits, and enabling technologies, IEEE Commun. Mag. 47 (11) (2009) 66–73.
[11] J. Leuthold, W. Freude, S. Sygletos, P. Vorreau, R. Bonk, D. Hillerkuss, I. Tomkos, A. Tzanakaki, C. Kouloumentas, D.J. Richardson, et al., An all-optical grooming switch to interconnect access and metro ring networks, in: 2008 10th Anniversary International Conference on Transparent Optical Networks, Vol. 3, IEEE, 2008, pp. 207–210.
[12] T. Sakirin, I. Asif, Infusing k-means for securing IoT services in edge computing, Mesop. J. Comput. Sci. 2023 (2023) 42–50.
[13] M. Jinno, Benefits of hierarchical spatial bypassing and spectral grooming in spatial channel networks, in: 2020 European Conference on Optical Communications, ECOC, IEEE, 2020, pp. 1–4.
[14] M. Jinno, Spatial channel network (SCN) architecture employing growable and reliable spatial channel cross-connects toward massive SDM era, in: 2018 Photonics in Switching and Computing, PSC, IEEE, 2018, pp. 1–3.
[15] Y. Asano, M. Jinno, Cost comparison of hierarchical optical cross-connect architectures for spatial channel networks (SCNs), in: 2018 Asia Communications and Photonics Conference, ACP, IEEE, 2018, pp. 1–3.
[16] M. Jinno, K. Yamashita, Y. Asano, Architecture and feasibility demonstration of core selective switch (CSS) for spatial channel network (SCN), in: 2019 24th OptoElectronics and Communications Conference (OECC) and 2019 International Conference on Photonics in Switching and Computing (PSC), IEEE, 2019, pp. 1–3.
[17] M. Jinno, T. Kodama, T. Ishikawa, Five-core 1× 6 core selective switch and its application to spatial channel networking, in: 2020 Optical Fiber Communications Conference and Exhibition, OFC, IEEE, 2020, pp. 1–3.
[18] M. Jinno, T. Kodama, T. Ishikawa, Principle, design, and prototyping of core selective switch using free-space optics for spatial channel network, J. Lightwave Technol. 38 (18) (2020) 4895–4905.
[19] M. Jinno, T. Ishikawa, T. Kodama, H. Hasegawa, S. Subramaniam, Enhancing the flexibility and functionality of SCNs: demonstration of evolution toward any-core-access, nondirectional, and contentionless spatial channel cross-connects, J. Opt. Commun. Netw. 13 (8) (2021) D80–D92.
[20] M. Yang, Q. Wu, M. Shigeno, Y. Zhang, Hierarchical routing and resource assignment in spatial channel networks (scns): Oriented toward the massive sdm era, J. Lightwave Technol. 39 (5) (2020) 1255–1270.
[21] M. Jinno, I. Urashima, T. Ishikawa, T. Kodama, Y. Uchida, Core selective switch with low insertion loss over ultra-wide wavelength range for spatial channel networks, J. Lightwave Technol. (2021).
[22] K. Nakada, H. Takeshita, Y. Kuno, Y. Matsuno, I. Urashima, Y. Shimomura, Y. Hotta, T. Sasaki, Y. Uchida, K. Hosokawa, et al., Single multicore-fiber bidirectional spatial channel network based on spatial cross-connect and multicore EDFA efficiently accommodating asymmetric traffic, in: Optical Fiber Communication Conference, Optica Publishing Group, 2023, pp. M4G–7.
[23] X. Yang, Q. Sun, Joint RMSSA scheme and link load balancing for static SD-SCNs from model building to algorithm design, J. Opt. Commun. Netw. 15 (8) (2023) 527–540.
[24] M. Jinno, Added value of introducing spatial bypass into WDM/SDM networks: Gaussian-noise model analysis for spatially-bypassed and spectrally-groomed optical channels, in: 2018 European Conference on Optical Communication, ECOC, IEEE, 2018, pp. 1–3.
[25] M. Jinno, Spatial channel cross-connect architectures for spatial channel networks, IEEE J. Sel. Top. Quantum Electron. 26 (4) (2020) 1–16.
[26] K. Harada, K. Shimizu, T. Kudou, T. Ozeki, Hierarchical optical path cross-connect systems for large scale WDM networks, in: Optical Fiber Communication Conference, Optica Publishing Group, 1999, p. WM55.
[27] A.A. Saleh, J.M. Simmons, Architectural principles of optical regional and metropolitan access networks, J. Lightwave Technol. 17 (12) (1999) 2431.
[28] X. Cao, V. Anand, C. Qiao, Framework for waveband switching in multigranular optical networks: part I-multigranular cross-connect architectures, J. Opt. Netw. 5 (12) (2006) 1043–1055.
[29] K. Ishii, H. Hasegawa, K.-i. Sato, M. Okuno, S. Kamei, H. Takahashi, An ultra-compact waveband cross-connect switch module to create cost-effective multi-degree reconfigurable optical node, in: 2009 35th European Conference on Optical Communication, IEEE, 2009, pp. 1–2.
[30] S. Sohma, T. Watanabe, N. Ooba, M. Itoh, T. Shibata, H. Takahashi, Silica-based PLC type 32 × 32 optical matrix switch, in: 2006 European Conference on Optical Communications, IEEE, 2009, pp. 1–2.
[31] Y. Uchida, T. Ishikawa, I. Urashima, S. Murao, T. Kodama, Y. Sakurai, R. Sugizaki, M. Jinno, Core selective switch supporting 15 cores per port using bundled three 5-core fibers, in: 2022 Optical Fiber Communications Conference and Exhibition, OFC, IEEE, 2022, pp. 01–03.
[32] Y. Uchida, I. Urashima, T. Ishikawa, S. Murao, K. Nakada, R. Tahara, Y. Sakurai, R. Sugizaki, M. Jinno, Design and performance of 1×8 core selective switch supporting 15 cores per port using bundle of three 5-core fibers, J. Lightwave Technol. 41 (3) (2023) 871–879.
[33] Edmund Optics, Edmund, 2023, https://www.edmundoptics.com/. (Accessed 18 June 2023).
[34] eBay, eBay, 2023, https://www.ebay.com/. (Accessed 18 June 2023).
[35] N. Nemoto, Y. Ikuma, K. Suzuki, O. Moriwaki, T. Watanabe, M. Itoh, T. Takahashi, 8×8 wavelength cross connect with add/drop ports integrated in spatial and planar optical circuit, in: 2015 European Conference on Optical Communication, ECOC, IEEE, 2015, pp. 1–3.
[36] L. Zong, P. Ji, T. Wang, O. Matsuda, M. Cvijetic, Study on wavelength cross-connect realized with wavelength selective switches, in: National Fiber Optic Engineers Conference, Optica Publishing Group, 2006, p. NThC3.
[37] K. Seno, A. Isoda, T. Mizuno, K. Yamaguchi, K. Suzuki, T. Hashimoto, Y. Miyamoto, 6× 6 wavelength cross connect with 2-f and 4-f optical systems for SDM photonic nodes, in: 2019 24th OptoElectronics and Communications Conference (OECC) and 2019 International Conference on Photonics in Switching and Computing (PSC), IEEE, 2019, pp. 1–3.
[38] J.M. Rivas-Moscoso, S. Ben-Ezra, P.S. Khodashenas, D.M. Marom, D. Klonidis, P. Zakynthinos, I. Tomkos, Cost and power consumption model for flexible super-channel transmission with all-optical sub-channel add/drop capability, in: 2015 17th International Conference on Transparent Optical Networks, ICTON, IEEE, 2015, pp. 1–4.
[39] M. Yang, Q. Wu, K. Guo, Y. Zhang, Evaluation of device cost, power consumption, and network performance in spatially and spectrally flexible SDM optical networks, J. Lightwave Technol. 37 (20) (2019) 5259–5272.
[40] W. Zheng, M. Yang, C. Zhang, Y. Zheng, Y. Zhang, Evaluation of optical transport unit line-card integration in spatially and spectrally flexible optical networks in terms of device cost and network performance, J. Lightwave Technol. 40 (19) (2022) 6319–6330.

[41] W. Zheng, M. Yang, C. Zhang, Y. Zheng, Y. Zhang, Robust design against network failures of shared backup path protected sdm-eons, J. Lightwave Technol. (2023).
[42] T. Matsui, T. Sakamoto, Y. Goto, K. Saito, K. Nakajima, F. Yamamoto, T. Kurashima, Design of 125 μm cladding multi-core fiber with full-band com-patibility to conventional single-mode fiber, in: 2015 European Conference on Optical Communication, ECOC, IEEE, 2015, pp. 1–3.
[43] H. Takara, A. Sano, T. Kobayashi, H. Kubota, H. Kawakami, A. Matsuura, Y. Miyamoto, Y. Abe, H. Ono, K. Shikama, et al., 1.01-Pb/s (12 SDM/222 WDM/456 Gb/s) crosstalk-managed transmission with 91.4-b/s/Hz aggregate spectral efficiency, in: European Conference and Exhibition on Optical Communication, Optica Publishing Group, 2012, pp. Th–3.
[44] M. Yang, C. Zhang, Q. Wu, W. Zheng, Y. Zhang, Comparison of switching policies in terms of switching cost and network performance in static SDM-EONs, Opt. Switch. Netw. 38 (2020) 100573.
[45] H. Yuan, M. Furdek, A. Muhammad, A. Saljoghei, L. Wosinska, G. Zervas, Space-division multiplexing in data center networks: on multi-core fiber solutions and crosstalk-suppressed resource allocation, J. Opt. Commun. Netw. 10 (4) (2018) 272–288.
[46] A.H. Wheeb, N.A.S. Al-Jamali, Performance analysis of OLSR protocol in mobile ad hoc networks, iJIM 16 (01) (2022) 107.
[47] A.H. Wheeb, D.N. Kanellopoulos, Simulated performance of SCTP and TFRC over MANETs: The impact of traffic load and nodes mobility, Int. J. Bus. Data Commun. Netw. (IJBDCN) 16 (2) (2020) 69–83.
[48] D. McGhan, W. Leckie, C. Chen, Reconfigurable coherent transceivers for optical transmission capacity and reach optimization, in: OFC/NFOEC, IEEE, 2012, pp. 1–3.
[49] A.H. Wheeb, M.T. Naser, Simulation based comparison of routing protocols in wireless multihop adhoc networks, Int. J. Electr. Comput. Eng. 11 (4) (2021) 3186.
[50] R. Rumipamba-Zambrano, J. Perelló, J.M. Gené, S. Spadaro, Cost-effective spatial super-channel allocation in Flex-Grid/MCF optical core networks, Opt. Switch. Netw. 27 (2018) 93–101.

Weichang Zheng received the B.S. degree in information and communication engineering from University of Electronic Science and Technology of China, Chengdu, China, in 2016, the M.S. degree and Ph.D. degree in policy and planning sciences from the University of Tsukuba, Tsukuba, Japan, in 2020 and 2023, respectively. He is currently working in University of Electronic Science and Technology as a postdoctoral. His research interests include optical networking, QoS routing, operations research, machine learning, and cloud computing.

Jinke Li received the B.S. degree in communication engineering from Jilin University, Changchun, China, in 2022, he is currently working toward the M.S. degree in communication engineering at the School of Information and Communication Engineering at the University of Electronic Science and Technology of China, Chengdu, China. His research interests include optical networking, Software defined networking, Intelligent information processing, Broadband wireless network, and mobile communication.

Ming Ke received his bachelor's degree in Electronic Information Engineering from North China University of Water Resources and Electric Power in 2022. He is currently pursuing a master's degree at the School of Information and Communication Engineering, University of Electronic Science and Technology of China. His current research interests include intelligent information processing, wireless communication, and optical networks.

Mingcong Yang received the B.S. degree in electrical and electronic engineering from Gunma University, Maebashi, Japan, in 2015, the M.S. degree and the Ph.D. degree in policy and planning sciences from the University of Tsukuba, Tsukuba, Japan, in 2017 and 2020, respectively. He is now working in Department of R&D,ZTE Corporation, Wuhan, China. His research interests include optical networking, operations research, machine learning, and cloud computing.

Yu Zheng received the B.E. degree in Digital media Technology from Ningbo University, Ningbo, China, in 2019, and he received the M.S. in policy and planning sciences at the University of Tsukuba, Japan, in 2022. He is currently working toward the Ph.D. degree with the Graduate School of Systems and Information Engineering, University of Tsukuba. His research interests include optical networking, Software defined networking, machine learning.

Chenxiao Zhang received his B.E. in the School of Electronics and Information at Northwestern Polytechnical University, China, in 2016, and he received the M.S.degree and Ph.D. degree in policy and planning sciences at the University of Tsukuba, Japan, in 2020 and 2023. Now, he is now working in KDDI Corporation, Tokyo, Japan. His main research interests are in the area of architectures of optical backbone networks, passive optical network and dynamic wavelength and bandwidth assignment schemes.

Qiang Liu (Member, IEEE) received the B.S., M.S., and Ph.D. degrees from the University of Electronic Science and Technology of China (UESTC), Chengdu, China, in 1996, 2000, and 2012, respectively.,After graduating from M.S. study, in 2000, he has worked with the School of Communication and Information Engineering, UESTC, where he is currently an Associate Professor. He had worked with the University of Essex, Colchester, U.K., from 2012 to 2013 and the University of California at Davis, Davis, CA, USA, from 2017 to 2018 as a Visitor Scholar. His research interests include wireless sensor networks, Internet of Things, broadband wireless networks, and molecular communication.,Dr. Liu is the Reviewer of IEEE Transactions on Nanobioscience and International Journal of Communication Systems. He is a member of IEEE ComSoc.

Yongbing Zhang received his B.S. in Electrical Engineering from Polytechnic University in 1984, and M.S. and Ph.D. degrees in Computer Science both from the University of Electro-Communications in 1989 and 1992. He was a Research Associate in the Department of Computer Science at the University of Electro-Communications from 1992 to 1996. He joined the Institute of Policy and Planning Sciences, University of Tsukuba as an Assistant Professor in 1996 and is now a Professor at the Graduate School of Systems and Information Engineering, University of Tsukuba. His research interests include distributed/parallel computer systems, communication networks, and performance evaluation. He is a member of IEEE.

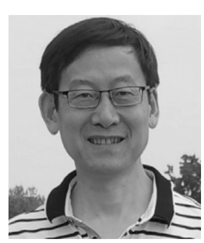

Kun Yang (Fellow, IEEE) received the Ph.D. degree from the Department of Electronic and Electrical Engineering, University College London, U.K. He is currently the Chair Professor with the School of Computer Science and Electronic Engineering, University of Essex, U.K., leading the Network Convergence Laboratory. He is also an Affiliated Professor with Nanjing University, China. He has managed research projects funded by UK EPSRC, EU FP7/H2020, and industries. He has published 400+ papers and filed 30 patents. His main research interests include wireless networks and communications, future Internet, and edge computing. In particular he is interested in energy aspects of future communication systems, such as 6G, promoting energy self-sustainability via both energy efficiency (green communications and networks), and energy harvesting (wireless charging). He serves on the editorial board of a number of IEEE journals (e.g., IEEE Transactions on Network Science and Engineering, IEEE Transactions on Vehicular Technology, and IEEE Wireless Communications Letters). He is a Deputy Editor-in-Chief of IET Smart Cities. He has been a Judge of GSMA GLOMO Award at World Mobile Congress – Barcelona since 2019. He was a Distinguished Lecturer of IEEE ComSoc from 2020 to 2021. He is a Member of Academia Europaea, a Fellow of IET, and a Distinguished Member of ACM.